JOURNAL OF MATERIALS SCIENCE 26 (1991) 3553–3564

Sintering and characterization of $Bi_4Ti_3O_{12}$ ceramics

C. JOVALEKIC
Center for Multidisciplinary Study, University of Belgrade, Slobodana Penezica 35/4, 11000 Belgrade, Yugoslavia

Lj. ATANASOSKA
Institute of Technical Sciences of Serbian Academy of Sciences and Arts, Belgrade, Yugoslavia

V. PETROVIC
The Faculty of Pedagogy and Techniques, Cacak, Yugoslavia

M. M. RISTIC
Serbian Academy of Sciences and Arts, Committee for Physical Chemistry, Belgrade, Yugoslavia

Polycrystalline ferroelectric $Bi_4Ti_3O_{12}$ ceramics have been prepared by the method of reactive liquid phase sintering. The sintering behaviour of the Bi_2O_3–TiO_2 composite was examined by plotting the isothermal densification curves. The results indicate that the starting oxides are involved in the reaction even at temperatures lower than or equal to 800 °C, but the reaction advances at a very slow rate. Above solidus, the liquid phase promotes an extended reaction. Saturation observed in two densification curves, at 875 and 1100 °C demonstrate that the reaction proceeds by two steps. A completion of the $Bi_4Ti_3O_{12}$ formation occurs after 60 min of sintering at 1100 °C. Optical micrographs of sintered bismuth titanate ceramics show randomly oriented ferroelectric grains separated by a paraelectric intergranular layer. The $Bi_4Ti_3O_{12}$ crystallites exhibit a platelike morphology, similar in the appearance to mica, as evidenced by scanning electron micrographs. Isothermal annealing (750 to 950 °C) does not affect the microstructure and electric properties of sintered bismuth titanate. The considerable value of dielectric permittivity and the appearance of hysteresis have been correlated to the presence of oxygen vacancies within the pseudotetragonal structure of $Bi_4Ti_3O_{12}$. The oxygen vacancies are preferentially sited in the vicinity of bismuth ions as evidenced by X-ray photoemission data. XPS and AES measurements confirm that the surface concentration of cations comprising the $Bi_4Ti_3O_{12}$ ceramics does not deviate from the nominal bulk composition.

1. Introduction

As a member of a large family of complex mixed Bi_2O_3–MeO ferroelectrics, bismuth titanate ($Bi_4Ti_3O_{12}$) is of particular interest due to its unique electro-optic switching behaviour. The potential for applications of bismuth titanate in memory storage and optical displays as piezomaterial and electrets has attracted scientific attention for its characterization at a fundamental level [1–9].

$Bi_4Ti_3O_{12}$ exists as a layer-type compound. Its structure is composed of a $Bi_2Ti_3O_{10}^{-2}$ layer, formed by two $BiTiO_3$ unit cells of hypothetical perovskite structure, alternating with a single $Bi_2O_2^{+2}$ layer [1, 2]. As do many other ferroelectrics, especially those in the perovskite family, bismuth titanate exhibits a phase change involving tilts in the oxygen octahedral chains. A reversible $\alpha \rightleftarrows \beta$ transition from an orthorhombic, ferroelectric form to a tetragonal paraelectric state takes place at the Curie temperature of 675 °C [2]. The high phase transformation point allows the application of $Bi_4Ti_3O_{12}$ within a wide temperature range.

Ferroelectrics are characterized by the anomalous behaviour of dielectric permittivity and specific conductivity in the vicinity of the Curie point [3]. The origin of the high magnitudes of dielectric permittivity and specific conductivity is closely related to polarization phenomena, space charge build up and relaxation either in the ferroelectric bulk or at the surface [4, 5]. Hysteresis loops observed in alternating field of high strength is associated with spontaneous polarization [6]. The dielectric anomalies of $Bi_4Ti_3O_{12}$ have been interpreted so far in the literature by phase transition [5], inhomogeneous distribution of electron space charges [7] and by the defect sites (impurities) in polycrystalline materials [6]. Sinjakov *et al.* [10] reported a formation of defects in the form of anionic vacancies.

0022–2461/91 $03.00 + .12

The main concern of the present study was to define sintering conditions for obtaining polycrystalline $Bi_4Ti_3O_{12}$ ceramics with the desired ferroelectric properties. In order to understand the electrical properties of the electrets it was crucial to examine in detail their microstructure, crystalline structure and chemical composition at the surface and in bulk. To accomplish this goal the results of Auger electron spectroscopy (AES), X-ray photoelectron spectroscopy (XPS), scanning electron (SEM) and optical microscopies were correlated with the electrical measurements. The surface region is expected to play an important role in the polarization phenomena of sintered $Bi_4Ti_3O_{12}$ ceramics. XPS is among the most suitable techniques to investigate the effects of surface layers on the electronic properties of materials [11]. The valence state of atoms comprising the binary oxide compound was identified by using XPS. The obtained data indicate that the oxygen vacancies are the major defect sites. The model for the oxygen vacancies distribution within the pseudotetragonal crystal structure of bismuth titanate is proposed. The polarization behaviour of the ceramics, sintered in this work, closely resembles that reported previously for the highly oriented polycrystalline bismuth titanate [12]. The values of the dielectric permittivity, coercive field, spontaneous and remanent polarization, determined for as-sintered samples, were not affected by the applied isothermal treatment (750 to 950 °C).

2. Experimental procedure

The polycrystalline $Bi_4Ti_3O_{12}$ ceramics were prepared by a method of reactive sintering. The standard ceramic fabrication procedure has been followed for the preparation of samples. The initial powders used in the present study were Bi_2O_3 (Bismuth Institute) and TiO_2 (GmbH Ventron) both at a purity of 99.8%. The two powders were mixed in the stoichiometric ratio (2:3) as required by the balance equation for a synthesis of the desired compound. The mixture was homogenized in agate ball mill for 1440 min, and then cold pressed under a compacting pressure of 50 MPa. After compression, the samples were sintered isothermally in air at 700 to 1100 °C for 30 to 240 min and then cooled down in the furnace to room temperature. The complete procedure has been repeated after cooling to get a final form of the $Bi_4Ti_3O_{12}$ ceramics. The specimens were re-ground in agate mill and recompacted to form pellets of the required size (a diameter of 9 mm, thickness of 1 mm). The twice ground and compacted powder of $Bi_4Ti_3O_{12}$ was again sintered at 1100 °C for 240 min. The sintered pellets were subjected to isothermal heat treatment within the temperature range from 750 to 950 °C for 60 to 240 min. The electrodes for the measurements of resistivity were applied to the polished surfaces of sintered discs by the screen printing method. The silver paste was polymerized at 600 °C for 30 min.

The microstructure of the chemically etched and fractured the $Bi_4Ti_3O_{12}$ ceramics pellets has been examined by light microscopy ("Reihert") and scanning electron microscopy. Electrical measurements were performed at room temperature. The dielectric permittivity was measured usually at a frequency of 1 kHz and a voltage (V_{rms}) of 1 V using LCZ automatic bridge (Hewlett-Packard 4276 A). Both, spontaneous and residual polarization, as well as the coercive field, were determined from a ferroelectric hysteresis loops observed by using a modified Sawer–Tower bridge circuit [13]. X-ray diffraction analysis was carried out with a Philips PW 1051.

The Auger spectra were recorded using the Riber cylindrical mirror analyser model OPC 105. The electron gun was mounted coaxially inside the CMA. The Auger electrons were excited by a primary electron beam of 2 keV energy at a normal incidence. The adsorbed beam current was 1.9 μm. The Auger signal was measured as peak-to-peak height in the EdN/dE mode. The modulation amplitude of the phase sensitive detector was set at 6 eV peak-to-peak. The Auger spectra were taken with the scan rate of 6 eV s^{-1}. A cleaning procedure was accomplished by sputter-etching with an Ar ion energy of 1 keV and an emission current density of 15 mA at an argon pressure of 6×10^{-3} Pa.

The XPS study were performed using a Perkin-Elmer Physical Electronics 555 Spectrometer (MgK_α X-ray source) with a PDP-11 computer for data acquisition and analysis. The relative surface composition of the $Bi_4Ti_3O_{12}$ ceramics was determined from the area of the Bi 4 f, Ti 2p and O 1s photoelectron peaks corrected by appropriate sensitivity factors [14]. Analysis of the core level spectra included background subtraction and iterative lineshape decomposition based on the summed Gaussian–Lorentzian functions. The calibration of the binding energy scale was checked using the C 1s line which appears in the photoelectron spectra of the as-received samples due to the common carbon contamination.

3. Results

3.1. Sintering behaviour

The insight into the propagation of the chemical reaction in the $2Bi_2O_3 + 3TiO_2$ composite during isothermal sintering of the $Bi_4Ti_3O_{12}$ compound can be gained by plotting densification curves. The apparent density was measured by the Archimedean method. The theoretical density of the composite was calculated from the equation

$$d = 1/[(1 - x)d_b + x/d_t]$$

where d_b (8.9 g cm^{-3}) and d_t (4.25 g cm^{-3}) are the specific gravities of Bi_2O_3 and TiO_2, respectively, and x is the weight fraction of TiO_2. The obtained theoretical value of 7.6 g cm^{-3} is almost twice the green density (4 g cm^{-3}) of the composite indicating very porous samples.

The densification behaviour for the sintering duration from 30 to 240 min in the temperature range of 700 to 900 °C is shown in Fig. 1a. The sintering densities at 700 °C do not differ from the green density and the time has no effect on the density level. The increase in sintering density occurs with increasing sintering temperatures. The densification at 800 °C is

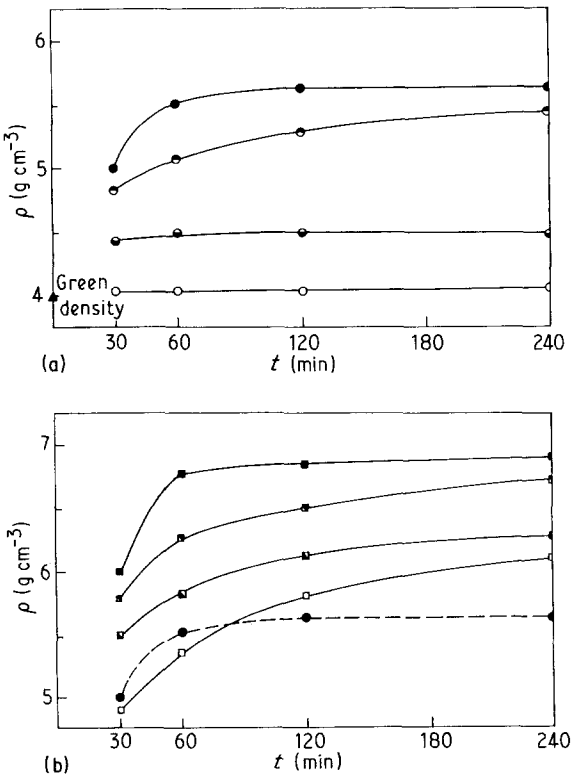

Figure 1 (a) The densification behaviour for the sintering duration from 30 to 240 min in the temperature range of 700 to 900 °C. (○ 700 °C, ◒ 800 °C, ◓ 850 °C, ● 875 °C). (b) The densification behaviour for the sintering duration from 30 to 240 min in the temperature range of 850 to 1100 °C. (● 875 °C, □ 950 °C, ◹ 1000 °C, ◹ 1050 °C, ■ 1100 °C).

only slightly affected by increase in sintering time. With further increase in sintering temperature a densification curve exhibits an evident slope. At 875 °C the apparent density reaches saturation after 60 min of sintering.

Above 875 °C there is a change in densification trend, as illustrated in Fig. 1b. A slight decrease in apparent density on sintering for less than 60 min is observed at 950 °C. For sintering times longer than 60 min the sintering density exceeds the saturation value at 850 °C and continues to increase approximately in a linear manner. Further elevation of temperature promotes densification. A set of nearly parallel densification curves is obtained at 950, 1000 and 1050 °C. At 1100 °C the rate of densification is very rapid within the initial 60 min of sintering. The saturation level is achieved after 60 min and the densification is accomplished.

The apparent density as a function of temperature for the constant sintering times is plotted in Fig. 2 for once- and twice-sintered samples. The curves for once-sintered samples exhibit well-defined plateau between 850 and 900 °C. The plateau is more pronounced for shorter sintering time (30 to 60 min). With increase in sintering duration the width of the plateau gradually narrows. No plateau appears in the case of twice-sintered samples.

The bulk of the ceramics, twice-sintered at 1100 °C, was characterized by X-ray diffraction method in order to check if the reaction of Bi_2O_3 and TiO_2 has been completed. All peaks observed in the obtained X-ray diffraction diagram in Fig. 3 belong to polycrystalline $Bi_4Ti_3O_{12}$ compound. This demonstrates that a synthesis has been successfully accomplished.

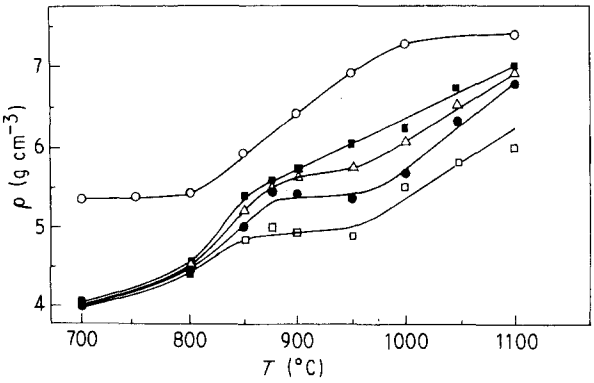

Figure 2 The apparent density as a function of temperature for the constant sintering times (once sintered: ○ 60 min; twice sintered: □ 30 min, ● 60 min, △ 120 min, ■ 240 min).

3.2. Auger electron spectroscopy data

The elements present in the surface region of as-sintered and thermally treated $Bi_4Ti_3O_{12}$ samples were identified qualitatively by Auger electron spectroscopy. A typical Auger spectrum in derivative mode recorded for $Bi_4Ti_3O_{12}$ ceramics is shown in Fig. 4. All peaks characteristic for bismuth, titanium and oxygen are clearly visible in the spectrum. The most intense Bi Auger signal for $N_5N_{6,7}N_{6,7}$ transition appears at 100 eV. The intensity ratio of two weaker bismuth peaks at 268 eV ($N_4O_3O_3$) and 249 eV ($N_5O_3O_3$) deviate slightly from the value given in the standard spectra for clean bismuth [15]. The Bi 268 eV peak in Fig. 4 is larger than the Bi 249 eV peak, in contrast to a known relative Auger yield of these two bismuth peaks. This indicates the presence of carbon impurity, because a carbon KLL transition at 270 eV partially overlaps with Bi ($N_4O_3O_3$) at 268 eV. A trace amount of carbon is detected after subtracting the contribution of bismuth from the total intensity of 268 eV peak. The spectrum reveals also traces of other common surface contaminants, sulphur and chlorine. The prominent Ti signals, for $L_2M_{2,3}M_{2,3}$ and $L_2M_{2,3}M_{4,5}$ Auger transitions, are located at 387 and 418 eV, respectively. The amplitude of the oxygen peak at 512 eV, for $KL_{2,3}L_{2,3}$ transition, exhibits a considerable intensity as expected for a specimen of a binary oxide compound. During the Auger measurements all peaks were shifted by 50 eV due to charging of the dielectric specimen, which required a recalibration of the electron energy scale.

Under our experimental conditions the Auger spectra were not reliable for a quantitative composition evaluation. The stoichiometry information derived from the Auger spectra is based on the measurements of the peak amplitudes corrected with the appropriate sensitivity factors. The Auger sensitivity factors were compiled for the energy of the primary electron beam of 3 keV [15]. In order to avoid charging problems, we had to reduce the energy of the primary beam from 3 to 2 keV as well as the adsorbed beam current. The modifications of the primary electron beam parameters during the AES experiments prevented use of

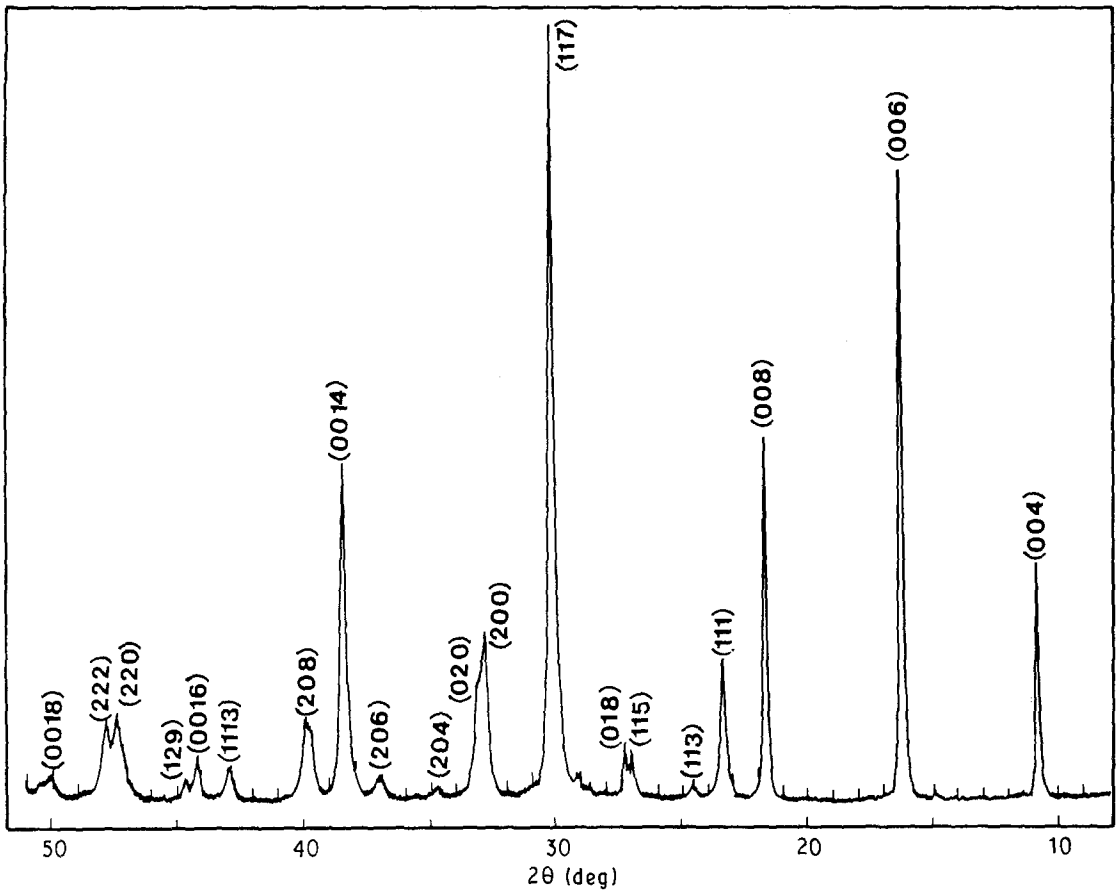

Figure 3 X-ray diffraction diagram of twice-sintered $Bi_4Ti_3O_{12}$ at 1100 °C.

established Auger sensitivity factors to arrive at an elemental composition estimate.

3.3. XPS data

The XPS survey spectrum of the "as-received" $Bi_4Ti_3O_{12}$ ceramics, prepared by reactive liquid phase sintering, is shown in Fig. 5. Beside the photoelectron lines characteristic of bismuth titanate, this spectrum demonstrate a presence of carbon impurities. The rigid shift (2.8 eV) of the valence bands and core levels was observed in a direction expected for ordinary photoemission-induced charging of the surface of dielectric specimens, i.e. positive charging of the surface.

Core level photoemission spectra were collected in order to obtain information on valence states of the elements constituting the bismuth titanate compound. The Bi 4f, Bi 5d, Ti 2p and O 1s core level photoemissions are shown in Fig. 6a to d. The 7/2 and 5/2 components of the Bi 4f spin–orbit doublet are located at 158.4 and 163.8 eV. The spin–orbit splitting of Bi 4f core levels for bismuth titanate compound is found to be in agreement with the standard value of 5.4 eV [14]. The ion etched samples exhibit a shoulder at low binding energy side of Bi 4f and Bi 5d photoemissions (Fig. 6a and b). The shoulder is attributed to the contribution of bismuth reduced to metallic state due to preferential cleavage of O–Bi bonds induced by incoming Ar ions followed by oxygen dissociation. Binding energy locations of the metallic bismuth $4f_{7/2}$ and $4f_{5/2}$ core levels, determined by lineshape deconvolution, are at 156.2 and 161.6 eV, respectively. The chemical shift of Bi 4f core levels for $Bi_4Ti_3O_{12}$ ceramics with respect to unreacted elemental bismuth is 2.2 eV, which is less than for the Bi_2O_3 compound (3.1 eV) [16, 17].

The Ti $2p_{1/2}$ photoemission is overlapped by the Bi $4d_{3/2}$ core level peak (Fig. 6c). The Ti $2p_{3/2}$ photoelectron peak which appears in the XPS spectrum as a distinctively resolved feature at the binding energy position of 459 eV unambiguously demonstrates the 4 + valence state of titanium atoms within the perovskite layer of bismuth titanate [18–20].

The lineshape of the O 1s core level photoemission reveals two peaks (Fig. 6d). The first one at low binding energy side corresponds to Ti–O bond while the second peak is ascribed to oxygen attached to bismuth. The oxygen atom in stronger Ti–O bond carries higher effective negative charge than in weaker Bi–O bond [21]. The correlation between the effective charge of oxygen atom and the binding energy of oxygen core electrons has been well documented in the literature [22].

The stoichiometry of the bismuth titanate compound has been estimated from the XPS spectra. The relative surface composition was determined from the measured area of core level peaks normalized by corresponding atomic sensitivity factors [14]. The same estimate of the composition has been obtained if the photoelectron peak areas were corrected for Scofield photoionization cross-sections [23]. The Bi:Ti atomic ratio was 4:3, which is in good agreement with the ideal stoichiometry of the bismuth titanate compound. The oxygen content is lower

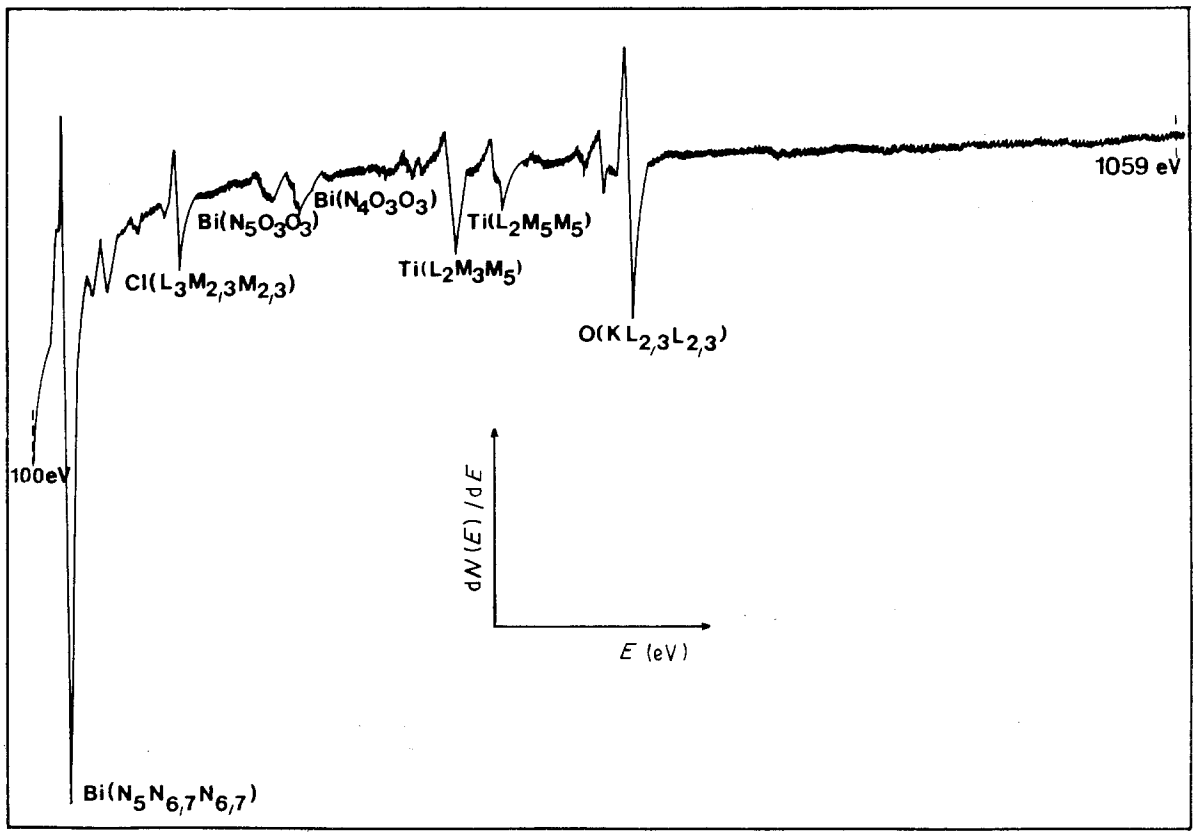

Figure 4 A typical Auger spectrum in derivative mode recorded for $Bi_4Ti_3O_{12}$ ceramics.

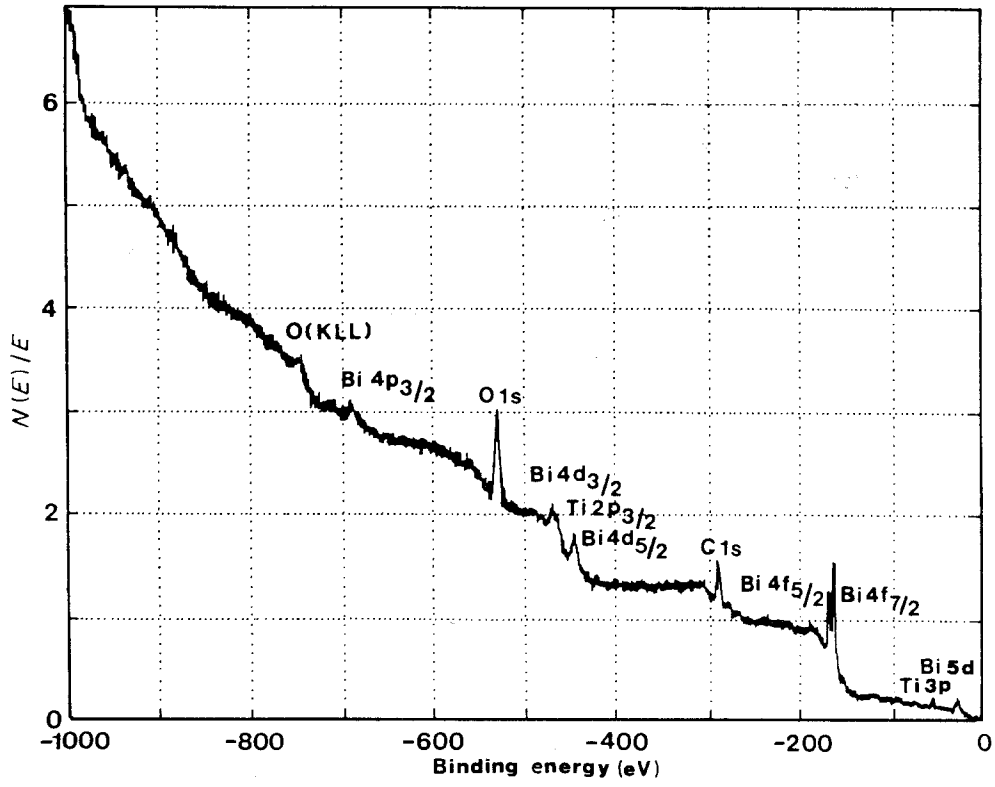

Figure 5 The XPS survey spectrum of the "as-received" $Bi_4Ti_3O_{12}$ ceramics, prepared by reactive liquid phase sintering.

by about 20% with regard to the nominal bulk composition.

3.4. Microstructure

The scanning electron micrographs in Fig. 7a and b demonstrate the morphology of starting oxides, the needle-like character of Bi_2O_3 and irregular round shape of TiO_2 particles. The microstructures of the $Bi_4Ti_3O_{12}$ ceramics, which were developed upon sintering at 750, 875, 950 and 1100 °C are shown in Figs 8 to 11. The phases of the starting oxides coexist with faintly developed plates for the sintering temperature of 750 °C as well as upon short sintering (30 min)

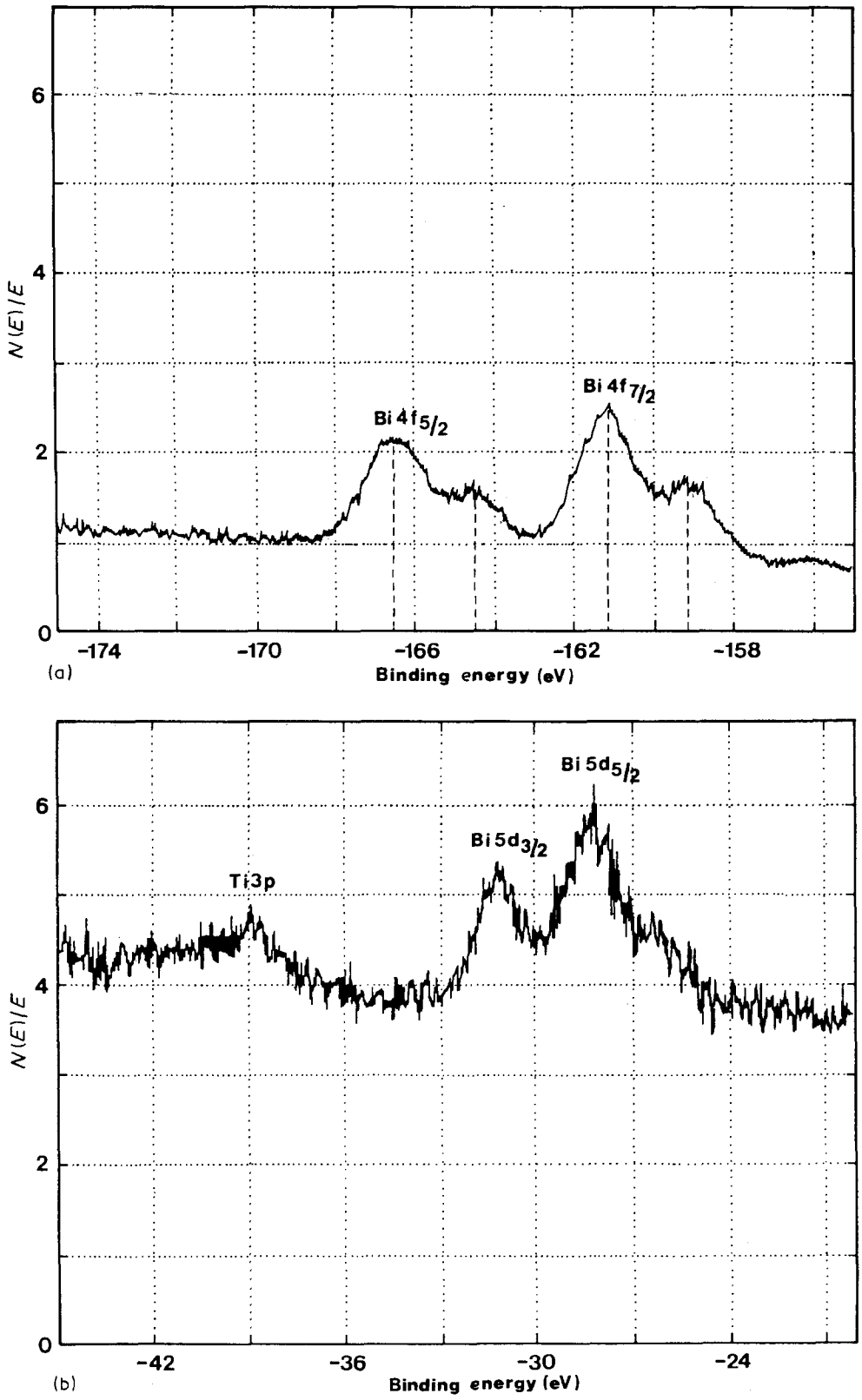

Figure 6 Core level photoemission spectra of twice-sintered bismuth titanate compound; (a) Bi 4f; (b) Bi 5d; (c) Ti 2p and (d) O 1s.

at 875 °C. Distinct plate-type texture appeared after 60 min of sintering at 875 °C. The most characteristic feature of the ceramics sintered at 950 °C for less than 60 min is the existence of many pores inside grains.

The scanning electron micrographs of the samples sintered at 1100 °C illustrates the presence of randomly distributed piles of thin plates of crystallite. The $Bi_4Ti_3O_{12}$ crystallites preferentially grow into a platelike shape, similar in a morphology to mica, due to a large anisotropy in surface energy [12, 24, 25]. The fine stripes in each thick grain of sintered bismuth titanate ceramics, always in parallel to the basal plane of the plates are clearly visible in the SEM photographs, as expected for the layer-type of structure. The same texture of platelike grains was previously observed and related to the crystal structure with Bi_2O_3 layers [26]. Even though the plates pile up in random orientations, the angles which most of them form with the compression axis do not diverge considerably from 90°. The regions with highly oriented plate-crystallites, normal to the compression axis, are also noticeable (Fig. 12). However these regions are scarce

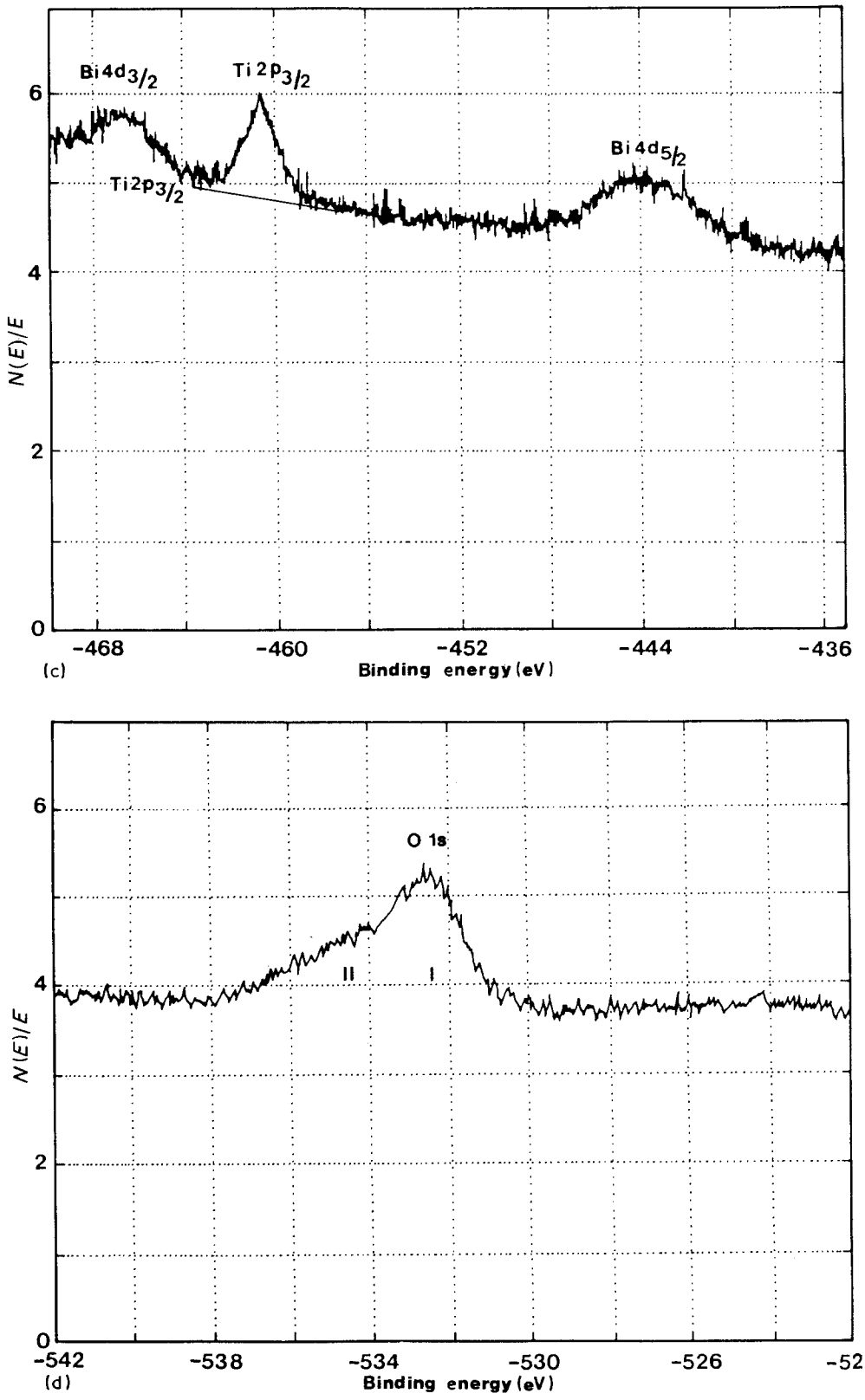

Figure 6 Continued.

and scattered. There is no apparent change in the size of plates upon isothermal annealing, in contrast to previous observations [25]. The optical micrographs, which show the fractured surfaces on a coarse scale, exhibit significant global similarities. A common feature of the microstructure, as seen by the optical microscope, is the presence of randomly oriented ferroelectric crystallites which are separated by paraelectric intergranular layer (Fig. 13a).

3.5. Dielectric measurements

An alternating electric field of high intensity was imposed on ceramic specimens of $Bi_4Ti_3O_{12}$ which were sintered at 1100 °C. Dielectric measurements were also performed on the sintered samples treated thereafter by isothermal annealing at 750, 850 and 950 °C. After subjection to fields provoking hysteresis, the values of coercive field, E_c, spontaneous polarization, P_s, and remanent polarization, P_r, were

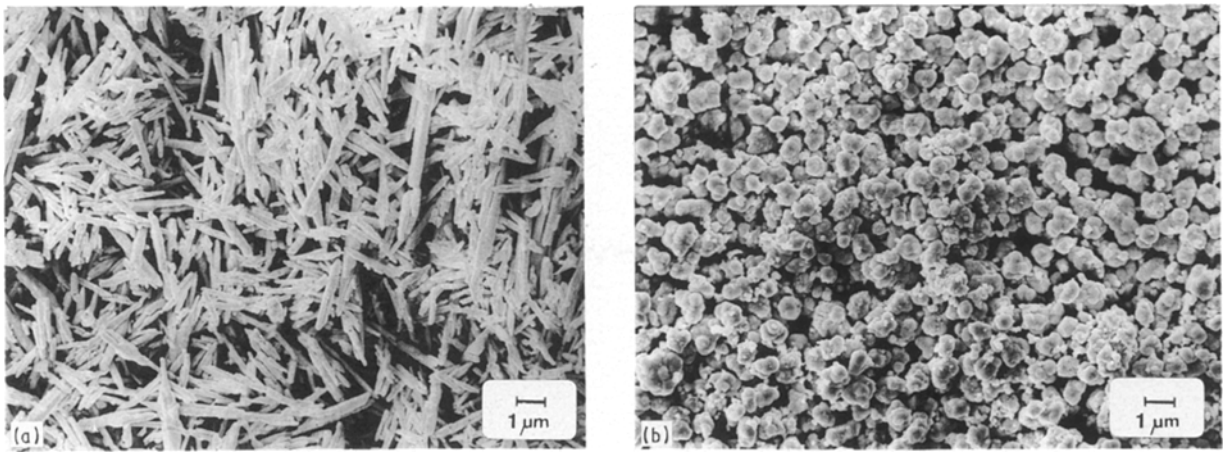

Figure 7 Scanning electron micrographs of starting oxides (a) Bi_2O_3; (b) TiO_2 particles.

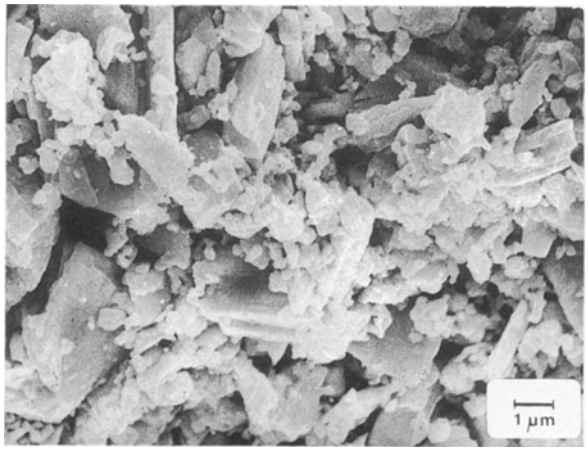

Figure 8 The microstructures of the $Bi_4Ti_3O_{12}$ ceramics, which were developed upon sintering at 750 °C.

determined by careful measurements of the loop parameters. The symmetric hysteresis loops were formed when the electric field of 3.3 MV m^{-1}, 50 c.p.s. was applied at room temperature (Fig. 13b). The average values of coercive field (E_c = 170 V m^{-1}), spontaneous (11 nC cm^{-2}) and remanent polarization (28 nC cm^{-2}) are lower than those of the bismuth titanate single crystal [2–8, 24]. The values were determined within 10% of the experimental accuracy.

The relative dielectric permittivities of the annealed $Bi_4Ti_3O_{12}$ ceramics were derived from the capacity measurements. The estimated value of 125 ± 5 is in agreement with that formerly reported for highly oriented polycrystalline samples, when measured in a direction of *c*-axis [12]. Dielectric permittivities measured after isothermal annealing treatment do not depart from the values determined for as-sintered samples. A drastic drop in dielectric permittivity value (by a factor of 10) occurs upon exposure to an oxidative atmosphere. Comparable deterioration in dielectric properties affected by oxidation treatment was previously reported for the $Bi_4Ti_3O_{12}$ single crystal, whose permittivity was reduced by a factor of 5 [27].

4. Discussion

The increase in apparent density of the composite with increasing sintering temperature from 700 to 800 °C is primarily caused by a decrease in porosity. The temperature elevation yields to faster migration and removal of the pores entrapped in the composite matrix. Despite the absence of measurable slope in the isothermal densification curves, which are almost horizontal lines for the temperatures lower and equal to 800 °C, the chemical reaction can not be excluded. The SEM photos (Fig. 8) demonstrate, besides the Bi_2O_3 needles and TiO_2 particles, the existence of small flaky shape grains, as an evidence of the initial stage of reaction on heating to temperatures close to and below the solidus. This is in general agreement with the results reported previously for the synthesis of the $Bi_4Ti_3O_{12}$ compound [25].

The reactive sintering at temperatures above the solidus occurs in the presence of the liquid phase. In the binary Bi_2O_3–TiO_2 system, the phase diagram shows that the formation of a liquid phase takes place at a minimum temperature of 825 °C [9]. The saturation level observed in two densification curves at 875 and 1100 °C (Fig. 1a and b) as well as the plateau around 875 °C which appears only in the case of once-sintered samples (Fig. 2) suggest that the reaction between the Bi_2O_3 and TiO_2 components proceeds in two steps. During the liquid phase sintering, the liquid is distributed by capillary forces, thus providing a favourable condition for the interaction of Bi_2O_3 with the TiO_2 particles. The liquid phase forms an easy path for material transport from one grain to another by solution and reprecipitation. At the temperatures slightly above 825 °C (by 50 to 60 °C) the amount of liquid phase is not sufficient to provide homogeneous distribution of the reactants. The departure from the 2:3 ratio of the reactive components in the composite allows the formation of other two Bi_2O_3–TiO_2 compounds predicted from the phase diagram beside $Bi_4Ti_3O_{12}$ [9]. The intermediate Bi–Ti–O compounds of the stoichiometry other than 4:3:12 are not stable. They have the melting point close to that of Bi_2O_3 and undergo transformation to the $Bi_4Ti_3O_{12}$ with progressive sintering.

At 875 °C the reaction is accomplished within initial 60 min. The prolongation of sintering has no effect on the density level attained at 60 min. This suggests that either the transport of the reactants is not efficient

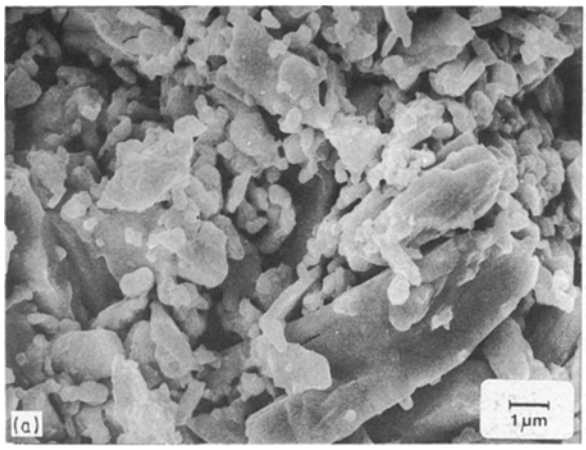

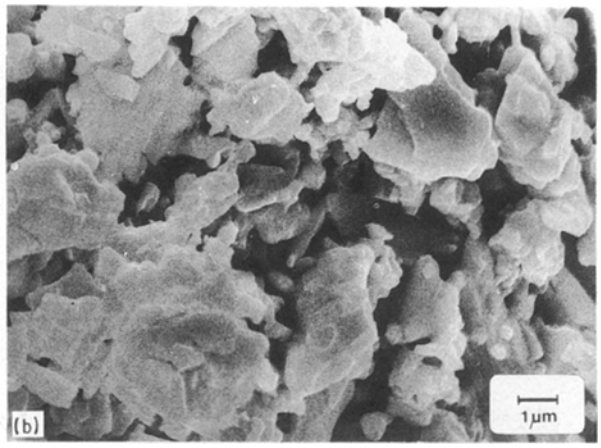

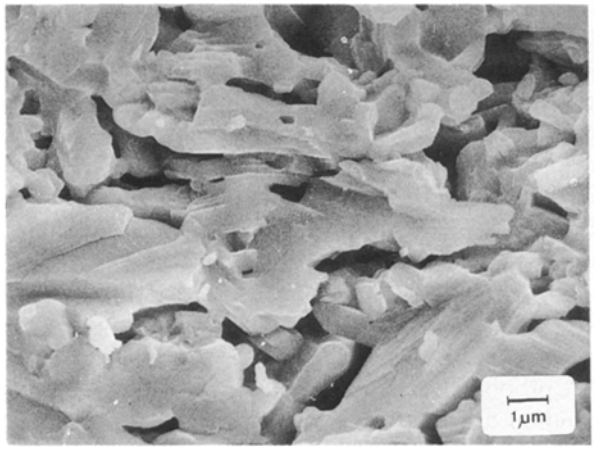

Figure 10 The microstructures of the $Bi_4Ti_3O_{12}$ ceramics, which were developed upon sintering at 950 °C.

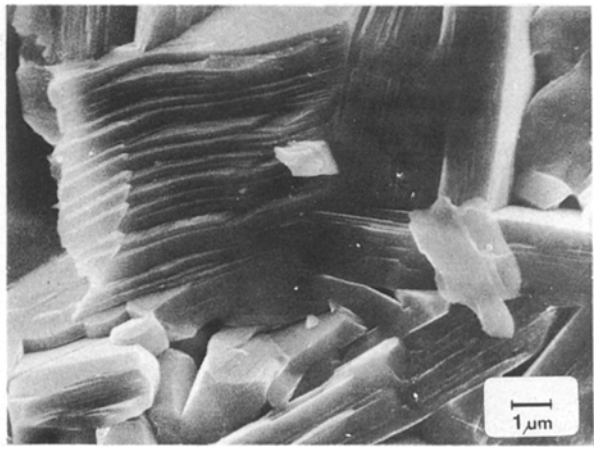

Figure 12 The regions with highly oriented platelike crystallites, normal to the compression axis.

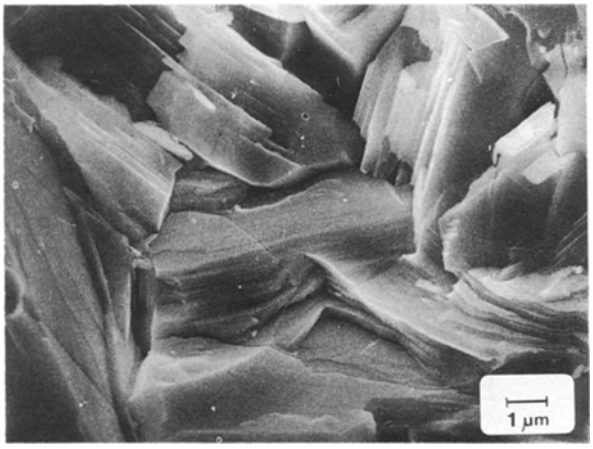

Figure 11 The microstructures of the $Bi_4Ti_3O_{12}$ ceramics, which were developed upon sintering at 1100 °C.

enough or the supply of liquid phase is insufficient for the extension and completion of the reaction. Probably the reaction products enclose the TiO_2 grains preventing further contact with the liquid Bi_2O_3 phase. Fig. 9a and b illustrate that the plate-like morphology of the ceramics, prepared at this temperature, is improved by extending the sintering time from 30 to 60 min.

The abrupt drop in the apparent density by sintering for less than 60 min at 950 °C is caused by the porous structure, as verified by SEM photos (Fig. 10). The pores developed during the cooling process of the excess of the liquid phase. The rate of reaction at this temperature is not high enough to consume the considerable amount of the liquid phase formed for short sintering times. As a result an excess of the liquid phase is present. With further elevation of temperature a complete homogenization is achieved and the enhanced content of the liquid phase is consumed more rapidly due to an adequate acceleration in the process of the reactive sintering. The support to this conclusion is the shrinkage of the plateau in the isothermal densification curves with increase in sintering time (Fig. 2). Extended sintering allows a consumption of the liquid phase at rates characteristic for the reaction around 950 °C.

The reaction is complete after 60 min of sintering at 1100 °C, as evidenced by a saturation in the isothermal densification curve, X-ray diffraction data and by the appearance of the large grains of the mica-like structure in the SEM photos. The platelike shape of the particles was a decisive factor in the orientation of the crystallite, yielding to the formation of stacks, piles arranged in layers. The majority of grains are a flaky shape with an average diameter about 5 μm and thickness up to 1 μm. This is in perfect agreement with previously observed grain sizes in grain oriented

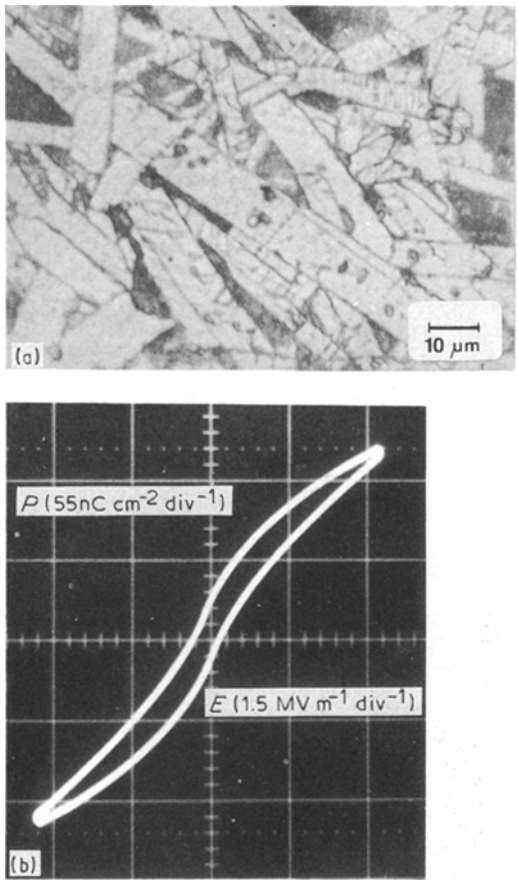

Figure 13 (a) Optical micrographs showing the presence of randomly oriented ferroelectric crystallites which are separated by paraelectric intergranular layer (b) The symmetric hysteresis loops were formed when the electric field of 3.3 MV m^{-1}, 50 c.p.s was applied at room temperature.

bismuth titanate [12, 28] and bismuth layer type ceramics [29].

The chemical shift of Bi 4f core level in the investigated $Bi_4Ti_3O_{12}$ ceramics was 2.2 eV with respect to metallic bismuth (Fig. 6a), which is less than for Bi_2O_3 (3 eV) [16, 17]. The observed shift could either be a characteristic of bismuth titanate or suggest the existence of bismuth in a valence state of $(+3-x)$. Both assumptions have support in the literature. Similar shifts to this observed in the present study has been reported for another bismuth compound, bismuth molybdate (1.5 to 2 eV) [30]. The valence state of bismuth lower than 3 + has, however, been detected by several authors, using various techniques. Dharmadhikari *et al.* [16, 17] have observed a significant difference by comparing the structural, electric and dielectric properties of the film obtained by direct vacuum evaporation of γ-Bi_2O_3 powder and the film annealed in the oxidation atmosphere. As-evaporated and oxidized films exhibited shifts in Bi 4f photoemission of ~ 2 and 3 eV, respectively, relative to pure bismuth metal. The shift of 2 eV was tentatively assigned by authors to a lower suboxide, BiO or Bi_2O_2, formed by dissociation of Bi_2O_3 during thermal evaporation. Dharmadhikari *et al.* [16] also found that the binding energy shift varies linearly with the oxidation state of Bi which further helped in identifying the nature of Bi in the suboxide. The results of electron diffraction measurements on thin bismuth oxide films grown by heating in air, in the early stage of bismuth oxidation, reported by Zav'yalova *et al.* [31] have identified oxides with lower stoichiometry than the crystallographically complicated Bi_2O_3 [32]. The formation of epitaxial BiO ordered overlayer was observed in LEED, AES and energy loss studies of oxygen interaction with bismuth single crystal [33].

Our data indicate a deficiency in oxygen. We have, therefore, attributed the shift of 2.2 eV in the Bi 4f region to bismuth in the sub-stoichiometric oxygen environment. The $Bi^{(+3-x)}$ formal oxidation state can be generated due to oxygen vacancies concentrated in the vicinity of bismuth cations either in the perovskite structure or in the Bi_2O_2 layer within the $Bi_4Ti_3O_{12}$ lattice. The oxygen vacancies neighbouring bismuth ion are more likely to be residing inside the Bi_2O_2 layer than in the hypothetical perovskite unit cell. In the perovskite portion of the $Bi_4Ti_3O_{12}$ structure the Bi ion is placed in the centre of the unit cell build by Ti cations. The oxygen anions form octahedra enclosing titanium ions. Bismuth and titanium cations share oxygen atoms. The outstanding affinity of Ti towards oxygen results in strong Ti–O bonds, which do not break easily and thus impede a formation of vacancies in the perovskite lattice.

No evidence of the valence state of Ti lower than 4 + is an additional support to the assumption about oxygen vacancies confinement to the Bi_2O_2 sequences. We propose that in the defect structure of $Bi_4Ti_3O_{12}$ a random distribution of oxygen vacancies is excluded and that acceptor dopants are existing within the Bi_2O_2 layers interleaved with the portions of perovskite-like structure (Fig. 14).

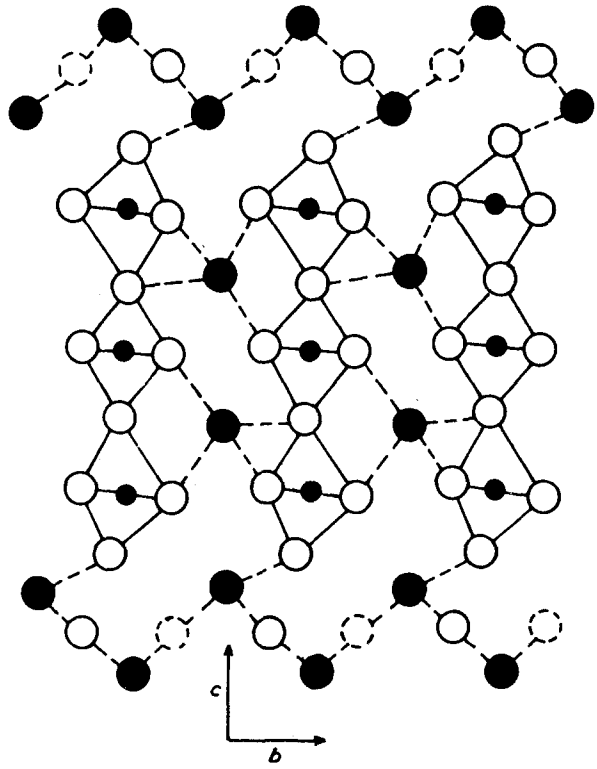

Figure 14 The proposed model for a defect structure of $Bi_4Ti_3O_{12}$ with oxygen vacancies confinement to the Bi_2O_2 layers interleaved with the portions of perovskite-like structure. (● Bi, ● Ti, ○ O, ○ oxygen vacancy).

Under the applied electric field the vacancies, whose presence is suggested by XPS data, migrate through the ceramic faster than they can be discharged or compensated at the electrode–dielectric interface. The accumulation of vacancies results in the appearance of migrational polarization. A drastic drop in dielectric permittivity value (by a factor of 10) which occurs upon exposure to an oxidative atmosphere can be explained by a reduction in migrational polarization. Previous suggestion of Ehara *et al.* [7], that the polarization of the electron cloud is induced across the potential barrier of the Bi_2O_2 layer can be questioned in the light of the present results. A space charge is generated due to the inhomogeneity in the high conductivity inside the volume and at the surface. The layer which contains high concentration of the acceptor dopants is not, however, likely to act as a potential barrier.

The polycrystalline bismuth titanate ceramics prepared in our experiments meet the basic requirements to be classified as ferroelectric. We have obtained hysteresis loops on polycrystalline samples at room temperature. So far a hysteresis behaviour of polycrystalline ceramics has been reported for elevated temperatures [34]. The loops at room temperature were observed only for hot-forged bismuth titanate ceramics [12]. Despite random crystallite orientations the estimated value of dielectric permittivity of 125 $\pm$ 5 is in surprising agreement with that formerly reported for highly oriented polycrystalline samples, when measured in the direction of *c* axis [12].

The existence of paraelectric intergranular layer inside the ceramics (Fig. 13a) accounts for the lower average values of coercive field, spontaneous and remanent polarization with respect to the bismuth titanate single crystal and highly oriented samples.

5. Conclusions

The method of reactive liquid phase sintering has been used to obtain the polycrystalline $Bi_4Ti_3O_{12}$ ceramics with ferroelectric properties. The isothermal densification curves combined with optical and scanning electron microscopy enabled an insight into the sintering behaviour of the Bi_2O_3–TiO_2 composite. The results indicate that the initial stage of the reaction occurs at temperatures close to and below solidus; sintering at temperatures above solidus promotes the reaction. The reaction proceeds by two steps as evidenced by the saturation level exhibited in two densification curves, at 875 and 1100 °C. The optical micrographs demonstrate that the texture of sintered ceramics is composed of randomly oriented ferroelectric grains which are separated by paraelectric intergranular layer. A plate-like morphology of the $Bi_4Ti_3O_{12}$ crystallites, similar in the appearance to mica, is confirmed by scanning electron micrographs. The isothermal annealing (750 to 950 °C) has no effect on the microstructure and electric properties of sintered bismuth titanate. The XPS data reveal the nominal valence state of bismuth lower than 3 + . The Ti cation is found to be only in the 4 + oxidation state. Based on the obtained results we can draw a conclusion that within the pseudotetragonal structure of $Bi_4Ti_3O_{12}$ the oxygen vacancies are preferentially sited in the vicinity of bismuth ions, i.e. most probably confined to the Bi_2O_2 layer. The measured value of dielectric permittivity and the appearance of hysteresis have been correlated to the presence of oxygen vacancies. The surface concentration of cations comprising the $Bi_4Ti_3O_{12}$ ceramics, estimated from the XPS measurements does not differ from the nominal bulk composition.

References

1. B. AURIVILLIUS, *Arkiv Kemi* **1** (1950) 499.
2. J. F. DORRIAN, R. E. NEWNHAM, D. K. SMITH and M. I. KAY, *Ferroelectrics* **3** (1971) 17.
3. G. W. TAYLOR, S. A. KENEMAN, A. MILLER and S. E. CUMMINS, *ibid.* **2** (1971) 11.
4. M. M. HOPKINS and A. MILLER, *ibid.* **1** (1970) 37.
5. A. FOUSKOVA and L. E. CROSS, *J. Appl. Phys.* **41** (1970) 2834.
6. G. W. TAYLOR, *Ferroelectrics* **1** (1970) 79.
7. S. EHARA, K. MURAMATSU, M. SHIMAZU, J. TANAKA, M. TSUKIOKA, Y. MORI, T. HATTORI and H. TAMURA, *Jpn J. Appl. Phys.* **20** (1981) 877.
8. E. C. SUBBARAO, *J. Phys. Chem. Solids* **23** (1962) 665.
9. E. I. SPERANSKAYA, I. S. REZ, L. V. KOZLOVA, V. M. SKORIKOV and V. I. SLOVOV, *Neorganicheskie Materiali* **1** (1965) 232.
10. E. V. SINJAKOV, E. F. DUDNIK, V. M. DUDA, V. A. PODOLSKI and M. A. GORFUNKEL, *Fizika tverdogo tela* **16** (1974) 1515.
11. D. BRIGGS and M. P. SEAH (Eds) "Practical Surface Analysis By Auger and X-Ray Photoelectron Spectroscopy" (John Wiley, New York, 1983).
12. T. TAKENAKA and K. SAKATA, *Jpn J. Appl. Phys.* **19** (1980) 31.
13. C. B. SAWYER and C. H. TOWER, *Phys. Rev.* **35** (1930) 269.
14. C. D. WAGNER, W. M. RIGGS, L. E. DAVIS and J. F. MOULDER in G. E. Muilenberg (Ed.), "Handbook of X-Ray Photoelectron Spectroscopy" (Perkin-Elmer, Physical Electronic Division, Eden Prairie, MN, 1978).
15. L. E. DAVIS, N. C. MacDONALD, P. W. PALMBERG, G. E. RIACH, R. E. WEBER, "Handbook of Auger Electron Spectroscopy" (PHI, Eden Prairie, MN, 1976).
16. V. S. DHARMADHIKARI, S. R. SAINKAR, S. BADRINARAYAN and A. GOSWAMI, *J. Electron. Spectrosc. Relat. Phenom.* **25** (1982) 181–189.
17. V. S. DHARMADHIKARI and A. GOSWAMI, *J. Vac. Sci. Technol.* **A1** (1983) 383–387.
18. G. B. HOFLUND, H.-L. YIN, A. L. GROGAN, Jr., D. A. Asbury, H. YONEYAMA, O. IKEDA and H. TAMURA, *Langmuir* **4** (1988) 346.
19. J. M. McKAY and V. E. HENRICH, *Surf. Sci.* **137** (1984) 463.
20. G. ROCKER and W. GOPEL, *ibid.* **181** (1987) 530.
21. O. KUBASCHEWSKI and C. B. ALCOCK, "Metallurgical Thermochemistry", 5th Edn (Pergamon, Oxford, 1979).
22. B. FOLKESSON and P. SUNDBERG, *Spectrosc. Lett.* **20** (1987) 193–200.
23. J. H. SCOFIELD, *J. Electron. Spectrosc. Relat. Phenom.* **8** (1976) 129–137.
24. S. E. CUMMINS and L. E. CROSS, *J. Appl. Phys.* **39** (1968) 2268.
25. T. KIMURA, T. KANAZAWA and T. YAMAGUCHI, *J. Amer Ceram. Soc.* **66** (1983) 597.
26. S. IKEGAMI and I. UEDA, *Jpn J. Appl. Phys.* **13** (1974) 1572.
27. V. A. PODOLSKI, E. F. DUDNIK and T. M. STOLPAKOVA, *Izv. Akad. Nauk USSR* **39** (1975) 1041.
28. H. WATANABE, T. KIMURA and T. YAMAGUCHI, *J. Amer. Ceram. Soc.* **72** (1989) 289.

29. W. XIAOLI and Y. XI, *Jpn J. Appl. Phys.* **24** (Suppl. 24–2) (1985) 1033.
30. J. ZHI-CHENG, AN LI-DUN and Y. YUAN-GEN, *Appl. Surf. Sci.* **24** (1985) 134.
31. A. A. ZAVYALOVA and R. M. IMAMOV, *Sov. Phys.-Crystallogr.* **13** (1968) 37 (Engl. transl.).
32. E. M. LEVIN and R. S. ROTH, *J. Res. NBS* **68A** (1964) 189.
33. T. N. TAYLOR, C. T. CAMPBELL, J. W. ROGERS, Jr., W. P. ELLIS and J. M. WHITE, *Surf. Sci.* **134** (1983) 529–546.
34. E. C. SUBBARAO, *Phys. Rev.* **122** (1961) 804.

Received 18 June
and accepted 26 June 1990